JOURNAL OF MATERIALS SCIENCE 30 (1995) 3668–3673

Fractal nature and quantitative evaluation of microstructures in metallic materials

M. TANAKA
Department of Mechanical Engineering, Mining College, Akita University 1-1, Tegatagakuen-cho, Akita 010, Japan

The fractal nature of microstructures was investigated using metallic materials containing second-phase particles, grain-boundary reaction (GBR) nodules or creep voids. The area fraction of the precipitates or the creep voids in the specimens was correlated with the scale of the analysis. The microstructures of these specimens exhibited a fractal nature between the lower and the upper critical scales, and could be regarded as the aggregate of the unit pattern with the size of the upper critical scale. The fractal dimension of a given microstructure was generally larger in specimens containing a larger area fraction of the second phase. The lower critical scale was close to the average size of second-phase particles or GBR nodules or the size of a large creep void. The upper critical scale, above which the area fraction of the precipitates or the creep voids did not show a scale dependence, was generally much larger than the average size and the average spacing of the precipitates, but it was almost the same as or a fair degree smaller than the grain size in specimens containing the second-phase particles or the GBR nodules. In the creep-ruptured specimens, the upper critical scale was much larger than the initial grain size and the grain size at rupture. The true area fraction of the second phase or the creep voids corresponding to the upper critical scale was also obtained.

1. Introduction

Mandelbrot *et al.* first reported the fractal nature of fracture surfaces in impact-loaded and fractured steels [1]. Similar results were obtained by other investigators on dynamically loaded and fractured metallic materials [2], tensile-ruptured steels [3], fatigued steels [4] and creep-ruptured metallic materials [5, 6]. Dauskardt *et al.* revealed that the values of the fractal dimension of the fracture surfaces are in the range between 1.0 and 1.3 [7], depending upon the fracture processes of the material. It was found previously [6] that the fractal dimension of the fracture surface profile was close to that of the grain boundary in creep-ruptured specimens of metallic materials, because high-temperature fracture occurred on grain boundaries in these materials. Thus, the fractal dimension of the fracture surfaces is associated with microstructures which are related to the fracture process.

Hornbogen reported that some kinds of microstructure in metals have a fractal nature [8]. A microstructure does not exhibit a fractal nature, if it is completely uniform. However, actual microstructures are generally neither completely uniform nor completely random, and some of them are expected to show a fractal nature in a certain scale range of the analysis in the estimation of the volume fraction of the second phase or the density of materials [8, 9]. Therefore, the fractal nature of microstructures can affect the quantitative evaluation of microstructural constituents, such as the area or volume fraction of second-phase particles or creep voids.

In this study, the effects of a fractal nature in microstructures on the estimation of the area fraction of the second phase or the creep voids were investigated using heat-treated and creep-ruptured specimens of metallic materials. The true area fraction of the precipitates or the creep voids and the critical scale of the analysis, above which a microstructure did not exhibit a scale dependence in the analysis, were also obtained.

2. Experimental procedure

Table I shows the chemical composition of the alloys used in this study. All the alloys were received in the form of round bars of about 20 mm diameter. The S80C carbon steel was heat treated in order to obtain a ferrite–cementite structure. The 21Cr–4Ni–9Mn steel was heat-treated to cause pearlitic grain-boundary reaction (GBR) nodules or solution treated at relatively low temperature to retain residual precipitates and a small grain size. A cobalt-base 20 W alloy was solution treated and aged to develop matrix precipitates of tungsten solid solution and carbide. Table II shows the microstructure and grain size in specimens of the alloys. Some heat-treated specimens of the 21Cr–4Ni–9Mn steel were machined into creep-rupture test pieces of 5 mm diameter and 30 mm gauge length. Creep-rupture experiments were carried out under a stress of 78.4 MPa at 1273 K in air. The

0022–2461

TABLE I Chemical composition of the alloys used in this study (wt %)

Alloy	C	N	Cr	Ni	Co	Fe	Mn	W	Si	S	P
21Cr–4Ni–9Mn steel	0.54	0.39	21.10	4.07	–	Bal.	9.74	–	0.19	0.008	0.017
20 W alloy	0.06	–	19.05	9.54	Bal.	2.28	0.77	19.74	0.19	0.001	0.003
S80C carbon steel	0.83	–	–	–	–	Bal.	0.48	–	0.21	0.004	0.011

TABLE II The microstructure and grain size in the heat-treated specimens of the alloys

Alloys	Heat treatments[a]	Microstructure	Grain diameter (m)
21Cr–4Ni–9Mn steel	1473 K, 3.6 ks, FC → 1173 K, 360 s → AC	Pearlitic GBR	9.9×10^{-5}
	1473 K, 3.6 ks, FC → 1173 K, 3.6 ks → AC	nodules in fcc	9.9×10^{-5}
	1573 K, 3.6 ks, FC → 1173 K, 3.6 ks → AC	matrix	3.1×10^{-4}
	1573 K, 3.6 ks, FC → 1173 K, 10.8 ks → AC		3.1×10^{-4}
	1573 K, 3.6 ks, FC → 1173 K, 10.8 ks → AC		
	1323 K, 1.8 ks → AC	Residual precipitates in fcc matrix	8.4×10^{-6}
20 W alloy	1573 K, 7.2 ks → WQ + 1273 K 1080 ks → AC	Tungsten solid solution and carbide particles in fcc cobalt matrix	2.73×10^{-4}
S80C carbon steel	1373 K, 3.6 ks → AC + 973 K, 180 ks → AC	Ferrite–cementite structure	7.8×10^{-5}

[a] FC, furnace-cooled; WQ, water-quenched; AC, air-cooled; GBR, grain-boundary reaction.

ruptured specimens were longitudinally sectioned for microscopic observations.

The heat-treated or ruptured specimens were finally polished with diamond paste of 1/4 μm in grain size and then electrolytically etched by 10% chromic acid in water. The microstructures of these specimens were examined using an optical microscope or a scanning electron microscope. Photomicrographs of the specimens were taken at the magnifications of ×50 to ×10000.

3. Analytical method

The total area of a set of second-phase particles or voids, $M(L)$, can be defined within a square of side length, L, on a photograph. If the distribution of the particles or the voids is uniform and plane-like, the value of $M(L)$ increases in proportion to L^2 with an increase of L [10]. In the general case, the distribution of the second phase or the voids can be characterized by the fractal dimension, D [10], such that

$$M(L) = M_0 L^D \quad (1)$$

where M_0 is a constant. Therefore, the area fraction of the particles or the voids, $A(L)$, within a square of side length, L, is expressed as [9]

$$A(L) = A_0 L^{D-2} \quad (2)$$

where A_0 is a constant.

Fig. 1 shows an example of patterns in which the area fraction of the second phase (displayed in black) is assumed to have a fractal nature in a limited scale range. For example, if the centre of squares for the analysis of area fraction (L_1, L_2, L_3) is taken inside a second-phase island, the area fraction of the second phase may show a scaling nature in a certain range of the scale of the analysis. When trying to find the fractal dimension of second-phase particles or voids, one problem is where to position the centres of a set of the squares [10]. In this study, three sets of data obtained by changing the position of the centre were averaged in order to determine the fractal dimension for each photograph. Relatively large second-phase particles, GBR nodules or creep voids were chosen to position the centres of a set of squares for the analysis. The area fraction of the second phase (precipitates) or voids was obtained by linear analysis [11]. If a

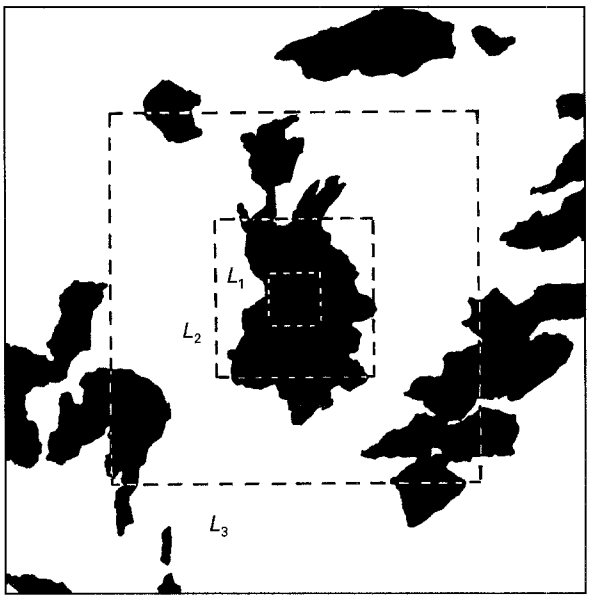

Figure 1 An example of microstructural patterns in a specimen containing black second-phase islands (L_1, L_2 and L_3 are squares in which the area fraction of the second phase is examined).

microstructural pattern has a fractal nature in the scale range between L^{**} and L^{*}, the fractal dimension of this pattern, D, can be obtained from Equation 2, such that

$$D = 2 - \log_{10} A^{*}/\log_{10}(L^{**}/L^{*}) \quad (3)$$

where A^{*} is the "scale-independent" true area fraction of the precipitates or the creep voids, L^{**} is the lower critical scale of the analysis corresponding to $A = 1$ and L^{*} is the upper critical scale corresponding to $A = A^{*}$. L^{*} is the critical scale above which the area fraction does not depend on the scale of the analysis.

4. Results and discussion

4.1. Area fraction of second-phase particles

Fig. 2 shows a scanning electron micrograph of a heat-treated specimen with ferrite-cementite structure in the S80C carbon steel. The average size and the average interparticle spacing of the spherical cementite particles are, respectively, about 7.6×10^{-7} and 1.9×10^{-6} m. The centres of three squares indicated in this figure are chosen for estimation of the area fraction of the cementite particles.

Fig. 3 shows the relationship between the area fraction of cementite particles, A, and the size of the square (the scale of the analysis), L, in the heat-treated specimen of the S80C carbon steel. The area fraction of cementite particles is 1.0 at very small scale of the analysis, L, and decreases with increasing value of L. Thus, the area fraction has a scale dependence (a fractal nature) between the lower critical size ($L^{**} = 5.1 \times 10^{-7}$ m) and the upper critical size ($L^{*} = 8.9 \times 10^{-6}$ m) of the square. The value of the fractal dimension, 1.265, is obtained using Equation 3. The area fraction finally becomes independent of the scale of the analysis, L, above L^{*} (8.9×10^{-6} m). The value of the abscissa corresponding to L^{*}, $A^{*} = 0.123$, gives the minimum value of A, namely, the "scale-independent" true area fraction of cementite particles. The value of L^{*} is about twelve times larger than the average radius of the cementite particles (about 7.6×10^{-7} m) and about five times larger than the interparticle spacing (about 1.9×10^{-6} m) in this specimen, although it is still less than the grain size (7.8×10^{-5} m). In this case, at least the area within a square of the size, L^{*} (8.9×10^{-6} m), should be examined in order to obtain the true area fraction of cementite particles. The value of L^{**} (5.1×10^{-7} m) is close to the average size of cementite particles.

Fig. 4 shows an optical micrograph of a cobalt-base 20 W alloy specimen containing ellipsoidal tungsten solid solution and carbide particles. The average particle size (approximated by the diameter of a round precipitate with the equivalent area) and the average interparticle spacing are, respectively, about 8.1×10^{-7} and 2.6×10^{-6} m. Three centres chosen for the analysis are also indicated in the figure. Fig. 5 shows the relationship between the area fraction of tungsten solid solution and carbide particles, A, and the scale of the analysis (the size of square), L, in the heat-treated specimen of the cobalt-base 20 W alloy.

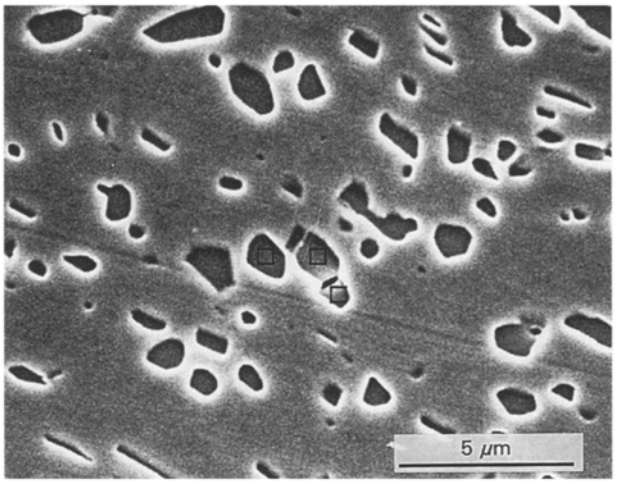

Figure 2 A scanning electron micrograph of a heat-treated specimen with ferrite–cementite structure in the S80C carbon steel (the centres of three squares chosen for the analysis are also shown in the figure).

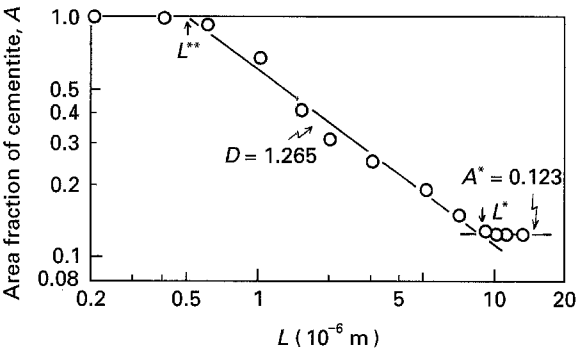

Figure 3 The relationship between the area fraction of cementite particles, A, and the size of the square (the scale of the analysis, L) in the heat-treated specimen of the S80C carbon steel.

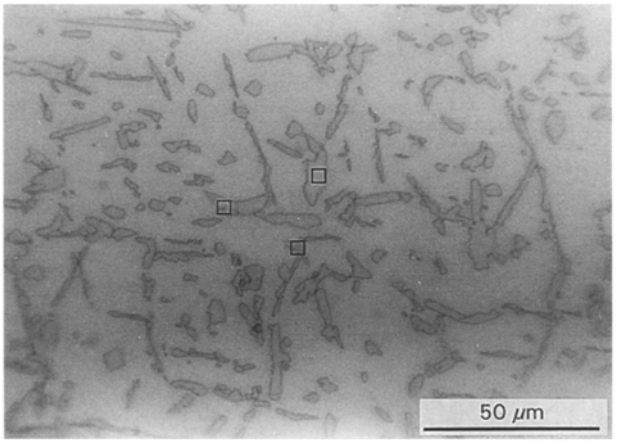

Figure 4 An optical micrograph of a heat-treated specimen of the cobalt-base 20 W alloy containing ellipsoidal tungsten solid solution and carbide particles (the centres of three squares chosen for the analysis are also shown in the figure).

The area fraction of the particles, A, decreases with increasing L. The fractal dimension of 1.403 was obtained in the range from $L^{**} = 1.1 \times 10^{-6}$ to $L^{*} = 2.4 \times 10^{-5}$ m. The area fraction is independent of the scale of the analysis, L, above the upper critical

value, L^* (2.4×10^{-5} m). This value is about thirty times larger than the average particle size (about 8.1×10^{-7} m) and about nine times larger than the interparticle spacing (about 2.6×10^{-6} m), but less than the grain size of the specimen (2.73×10^{-4} m). The true area fraction corresponding to L^*, A^* is 0.156 in this case. The value of L^{**} is close to the average particle size of the precipitates.

Thus, the value of L^* is a fair degree larger than the interparticle spacing of the second-phase particles in these specimens. These results show that the microstructural patterns have a fractal nature in a certain scale range of the analysis, L, in these specimens.

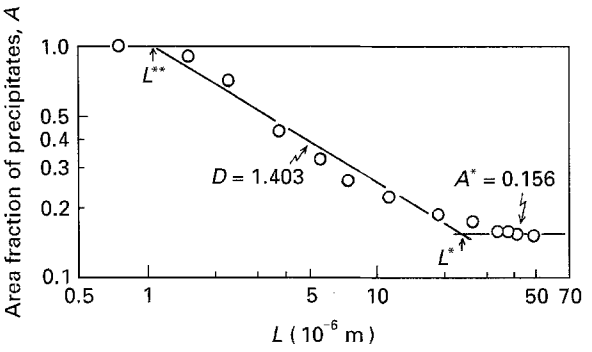

Figure 5 The relationship between the area fraction of tungsten solid solution and carbide particles, A, and the scale of the analysis, L, in the heat-treated specimen of the cobalt-base 20 W alloy.

4.2. The amount of grain-boundary reaction (GBR)

Fig. 6 shows optical micrographs of specimens solution treated and aged at 1173 K in the 21Cr–4Ni–9Mn steel. Spherical pearlitic nodules (cellular precipitates) are formed by the grain-boundary reaction (GBR) in this steel. The GBR nodules grow from one side or both sides of grain boundaries (for example, Fig. 6a and b). The growth of the GBR nodules ceases where the nodules meet other nodules or grain boundaries and seems to be restricted within one grain. The average size of the GBR nodules is about 2.7×10^{-5} to 3.3×10^{-5} m in the specimens with a grain diameter of 9.9×10^{-5} m and about 3.7×10^{-5} to 6.2×10^{-5} m in the specimens with a grain diameter of 3.1×10^{-4}m, while the average spacing between the GBR nodules is about 4.1×10^{-5} to 4.6×10^{-5} m for the former specimens and about 8.0×10^{-5} to 9.3×10^{-5} m for the latter specimens. The amount of GBR means the area fraction of the GBR nodules in this study. The number of GBR nodules and the average size of the nodules are larger and the average spacing between the GBR nodules is smaller in specimens with a larger amount of GBR (for example, Fig. 6b and d). The centres of squares chosen for the analysis of the amount of GBR are also shown in Fig. 6.

Fig. 7 shows the relationship between the amount of GBR, A, and the scale of the analysis, L, in the solution-treated and aged specimens with a grain diameter of 9.9×10^{-5} m. The amount of GBR is 1.0 at the very

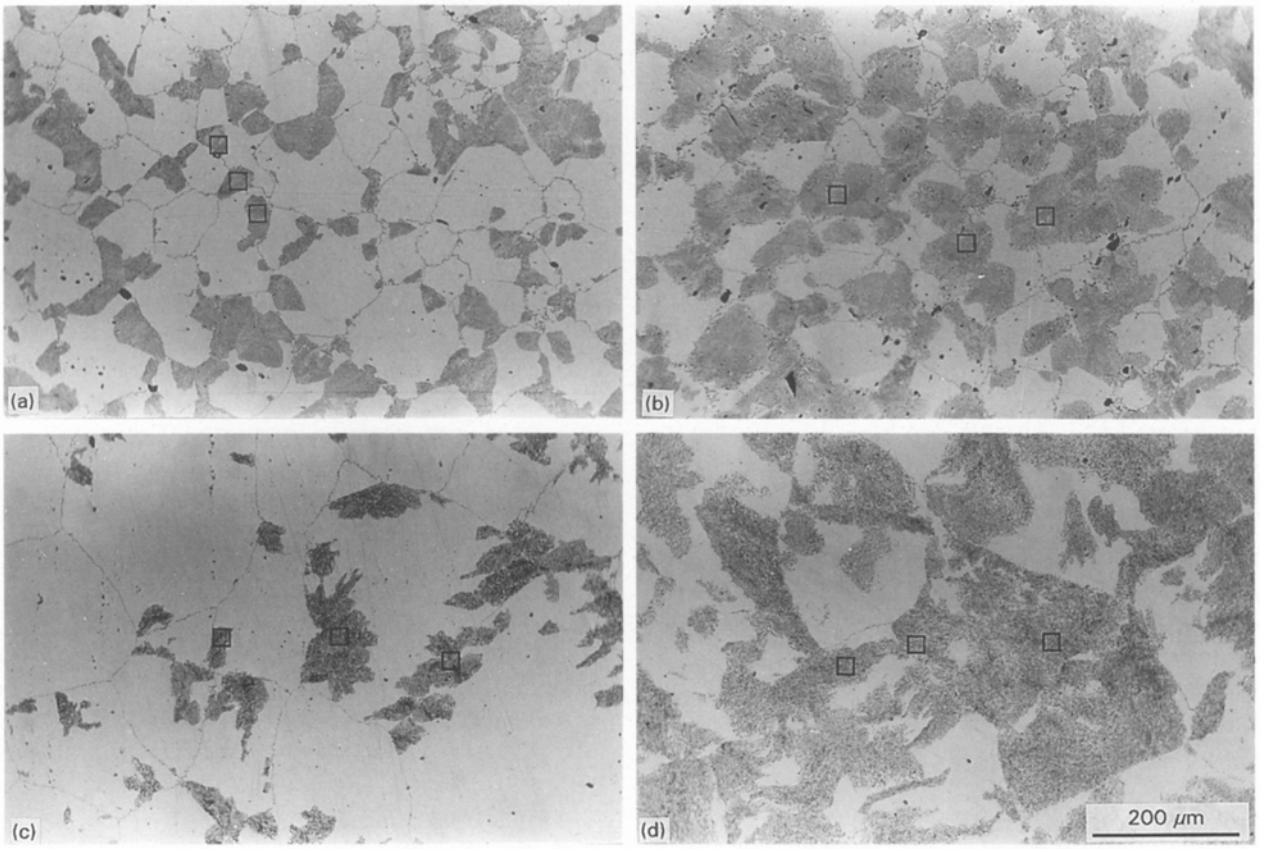

Figure 6 Optical micrographs of specimens solution-treated and aged at 1173 K in the 21Cr–4Ni–9Mn steel (the centres of three squares chosen for the analysis are also shown in the figure): (a) aged for 360 s at 1173 K ($d = 9.9 \times 10^{-5}$ m); (b) aged for 3.6 ks at 1173 K ($d = 9.9 \times 10^{-5}$ m); (c) aged for 3.6 ks at 1173 K ($d = 3.1 \times 10^{-4}$ m); (d) aged for 10.8 ks at 1173 K ($d = 3.1 \times 10^{-4}$ m), where d is the grain diameter.

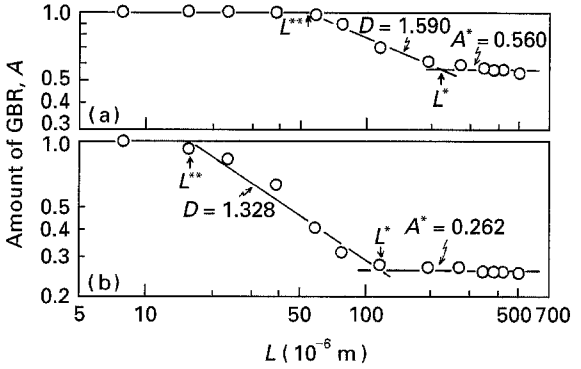

Figure 7 The relationship between the amount of the grain-boundary reaction (GBR), A, and the scale of the analysis, L, in the heat-treated specimens with the grain diameter of 9.9×10^{-5} m of the 21Cr–4Ni–9Mn steel: (a) aged for 360 s at 1173 K; (b) aged for 3.6 ks at 1173 K.

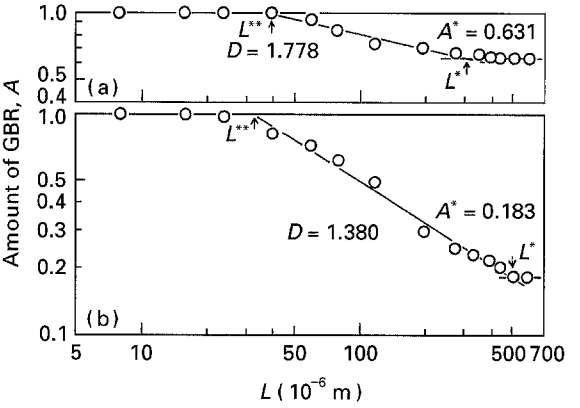

Figure 8 The relationship between the amount of the grain-boundary reaction (GBR), A, and the scale of the analysis, L, in the heat-treated specimens with the grain diameter of 3.1×10^{-4} m of the 21Cr–4Ni–9Mn steel: (a) aged for 3.6 ks at 1173 K; (b) aged for 10.8 ks at 1173 K.

small scale of analysis, L, but shows a scale dependence between the lower critical scale, L^{**}, and the upper critical one, L^*. The amount of GBR is independent of the scale of the analysis above a certain value of L, L^*. The value of A^* shows the true amount of GBR obtained for the two specimens. The value of L^{**} is close to the average size of the GBR nodules. The fractal dimension, D, estimated using Equation 3 is 1.590 in the scale range between $L^{**} = 5.5 \times 10^{-5}$ m and $L^* = 2.2 \times 10^{-4}$ m of the square for the specimen of $A^* = 0.560$ (Fig. 7a) and 1.328 in the scale range between $L^{**} = 1.6 \times 10^{-5}$ m and $L^* = 1.2 \times 10^{-4}$ m for the specimen of $A^* = 0.262$ (Fig. 7b). The fractal dimension, D, and the value of L^* are larger in the specimen with the larger amount of GBR, A^* (Fig. 7a). The values of L^* are about four to seven times larger than the average size of GBR nodules and about three to five times larger than the average spacing of the GBR nodules, but the same as or twice as large as the grain size of these specimens (9.9×10^{-5} m).

Fig. 8 shows the relationship between the amount of GBR, A, and the size of square used for the analysis, L, in the solution-treated and aged specimens with the grain diameter of 3.1×10^{-4} m. The amount of GBR decreases with an increase in the scale of the analysis, L, in the intermediate range of L. The fractal dimension obtained using Equation 3 is 1.778 in the scale range from $L^{**} = 3.9 \times 10^{-5}$ to $L^* = 3.1 \times 10^{-4}$ m for the specimen of $A^* = 0.631$ (Fig. 8a) and 1.380 in the scale range between $L^{**} = 3.3 \times 10^{-5}$ and $L^* = 5.0 \times 10^{-4}$ m for the specimen of $A^* = 0.183$ (Fig. 8b). The value of D is larger in the specimen with the larger amount of GBR (Fig. 8b). The values of L^* are about five to fourteen times larger than the average size of GBR nodules and about four to five times larger than the average spacing between the GBR nodules, but the same as or twice as large as the grain size of these specimens (3.1×10^{-4} m).

As described above, the growth of the GBR nodules is affected by other nodules in the same grain or in the neighbouring grains and is restricted within one grain by the presence of other nodules or grain boundaries. This is why the value of L^* is almost the same as the grain diameter of specimens, while the value of L^{**} is close to the average size of the GBR nodules. These results indicate that a microstructural pattern formed by the GBR nodules have a fractal nature in a limited scale range of the analysis. The area fraction of the second-phase particles or the GBR nodules in these specimens should be estimated by averaging the data obtained on several micrographs taken on different areas in the same specimen, but the minimum area which should be examined on each micrograph is given by a square area with the side length of L^*.

4.3. Area fraction of creep voids

Fig. 9 shows an optical micrograph of a specimen ruptured under a stress of 7.84 MPa at 1273 K. The tensile direction is horizontal in the micrograph. This part is about 6 mm apart from the fracture surface. The rupture life was 518 ks and the elongation was 0.957. Also shown are the centres of three squares used for the analysis of the area fraction of the creep voids. Many small voids and several large crack-like voids which were probably formed by the growth and linkage of small voids can be seen on grain boundaries. Some voids extend in the direction perpendicular to the tensile axis. A small amount of residual precipitate is also visible in the figure. Grain growth occurred during creep in this specimen, and the grain diameter increased from 8.4×10^{-6} m to 5.5×10^{-5} m at rupture. In spite of extensive grain growth during creep, a large elongation (0.957) was obtained in the fine-grained specimen (initial grain diameter 8.4×10^{-6} m) of the 21Cr–4Ni–9Mn steel containing residual precipitates under a low-stress and high-temperature condition. The sizes of most creep voids are in the range from about 8×10^{-7} m to about 8×10^{-5} m.

Fig. 10 shows the relationship between the area fraction of creep voids and the scale of the analysis in a specimen ruptured under a stress of 7.84 MPa at 1273 K. The area fraction of the creep voids decreases with an increase in the scale of the analysis in the range between $L^{**} = 2.3 \times 10^{-5}$ m and $L^* = 2.6 \times 10^{-4}$ m, and the fractal dimension, 0.704, is obtained by using Equation 3. The area fraction of the voids, $A^* = 0.0451$, which corresponds to the upper critical size of the square ($L^* = 2.6 \times 10^{-4}$ m) is also shown in the figure. More than thirty creep voids are

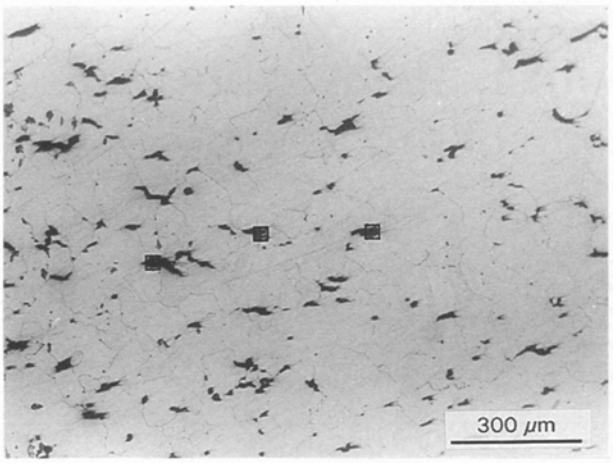

Figure 9 An optical micrograph of a ruptured specimen of the 21Cr–4Ni–9Mn steel crept under a stress of 7.84 MPa at 1273 K (rupture life = 518 ks, elongation = 0.957) (the centres of three squares chosen for the analysis are also shown in the figure).

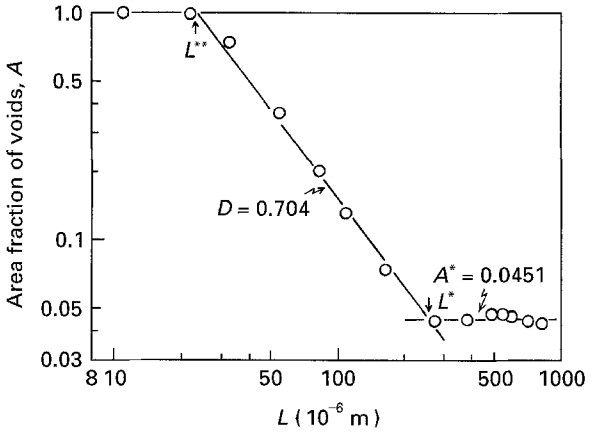

Figure 10 The relationship between the area fraction of creep voids, A, and the size of square (the scale of the analysis, L) in a specimen of the 21Cr–4Ni–9Mn steel ruptured under a stress of 7.84 MPa at 1273 K.

observed within a square of the side length of L^* with an optical microscope at the magnification of $\times 400$. The value of L^* is about fifty times larger than the initial grain diameter, and is about seven times larger than the grain diameter at rupture, while the lower critical scale, L^{**}, is close to a large creep void. Thus, a microstructural pattern formed by creep voids may have a fractal nature in a limited scale range of the analysis, L, in this specimen.

Microstructures containing precipitates or creep voids can be regarded as the aggregate of a unit pattern with the size of L^*. This indicates in statistical meaning that complex microstructures can be reproduced by the simple repetition of the unit microstructure. In this sense, the lower critical scale, L^{**}, and the upper critical scale, L^{**}, of the analysis and the true area fraction, A^*, of precipitates or creep voids, as well as the fractal dimension, D, of a microstructural pattern are important parameters characterizing the fractal nature of microstructures. The knowledge of a fractal nature in microstructures is applicable to the exploitation and design of materials, but it is necessary to know in further study the quantitative relationship between the fractal nature of microstructural patterns and the material properties such as mechanical, physical and chemical properties before the application.

5. Conclusions

The fractal nature of microstructures was studied on metallic materials containing second-phase particles, grain-boundary reaction (GBR) nodules or creep voids. The area fraction of the precipitates or the creep voids was correlated with the scale of the analysis. The results obtained may be summarized as follows.

1. The microstructures of these specimens exhibited a fractal nature between the upper and lower critical scales. The microstructures could be regarded as an aggregate of the unit pattern with the size of the upper critical scale. The true area fraction of the precipitates or the creep voids, which corresponded to the upper critical scale, was obtained by plotting the area fraction of the second phase or the creep voids against the scale of the analysis. The fractal dimension of a given microstructure was generally larger in the specimens containing a larger area fraction of precipitates.

2. In the specimens containing second-phase particles or GBR nodules, the lower critical scale was close to the average size of the particles or the nodules and the upper critical scale was generally much larger than the average size and the average spacing of these precipitates. This scale was a fair degree smaller than the grain size in the specimens containing fine precipitate particles, but it was almost the same as the grain size in the specimens in which the GBR nodules were formed.

3. In the specimen containing creep voids, the lower critical scale was close to the size of a large creep void. The upper critical scale, above which the area fraction of creep voids did not exhibit a scale dependence, was much larger than the initial grain size and the grain size at rupture in this specimen.

References

1. B. B. MANDELBROT, D. E. PASSOJA and A. J. PAULLAY, *Nature* **308** (1984) 721.
2. C. S. PANDE, L. E. RICHARDS, N. LOUAT, B. D. DEMPSEY and A. J. SCHWOEBLE, *Acta Metall.* **35** (1987) 1633.
3. E. E. UNDERWOOD and K. BANERJI, *Mater. Sci. Eng.* **80** (1986) 1.
4. Z. W. WANG, D. L. CHEN, X. X. JIANG, S. H. ALI and C. H. SHIH, *Scripta Metall.* **22** (1988) 827.
5. M. TANAKA and H. LIZUKA, *Z. Metallkde* **82** (1991) 442.
6. M. TANAKA, *J. Mater. Sci.* **27** (1992) 4717.
7. R. H. DAUSKARDT, F. HAUBENSAK and R. O. RITCHIE, *Acta Metall.* **38** (1990) 143.
8. E. HORNBOGEN, *Int. Mater. Rev.* **34** (1989) 277.
9. D. STAUFFER and H. E. STANLEY, "From Newton to Mandelbrot," translated by S. Miyajima and H. Nishihara (Asakura Book Publishers, Tokyo, 1993) p. 197.
10. H. TAKAYASU, "Fractals in the physical sciences," (Manchester University Press, Manchester, New York, 1990) p. 16.
11. C. S. SMITH and L. GUTTMAN, *Trans. AIME* **197** (1953) 81.

Received 15 December 1993
and accepted 3 February 1995